A model of the backside illuminated Chandra CCD.

Gregory Prigozhin, Mark Bautz, George Ricker

Center for Space Research, Massachusetts Institute of Technology,
Cambridge, Massachusetts

ABSTRACT

In this work we describe a simulator developed to model the X-ray response of the backside illuminated Chandra CCDs. The model is based on the Monte-Carlo technique, where individual X-ray photons are thrown into the silicon structure and the behavior of the simulated electron clouds is calculated. In order to reproduce the complex redistribution function of the device at low energies we had to introduce charge losses for the clouds formed near the illuminated surface.

An important feature of this model is its simulation of Charge Transfer Inefficiency (CTI), which attempts to reproduce losses of signal charge to electron traps in the buried channel of the device during different vertical and horizontal charge transfers. The CTI model takes into account a reduction of the number of empty traps in the channel due to precursor charge packets found in the previous rows of the image section of the device.

Parameters of the model were tuned to fit the large amount of experimental data acquired during the on-the-ground calibration of the Chandra devices at energies ranging from 277 eV to 9.9 keV.

Keywords: X-ray, charge coupled device, charge transfer inefficiency, electron traps

1. INTRODUCTION

The focal plane of the ACIS (Advanced CCD Imaging Spectrometer) instrument aboard the Chandra X-ray Observatory contains 10 CCDs. Two of these are back side illuminated (BI) devices. BI CCDs have most of the bulk of the silicon substrate removed by chemical etching and are mounted with the remaining 40 microns of silicon looking in the direction of incoming X-ray photons. Unlike the frontside illuminated (FI) devices, the photons do not have to go through the gate structure of the CCD. As a result, the quantum efficiency of these devices is much higher, especially for low energy X-rays below 1 keV.

In order to properly analyze of the observatory-produced data one needs to know the response function of the detectors at any given monochromatic energy. This makes it possible to extract the spectral composition of the incoming X-ray flux from the data. An accurate model of the detector is required to produce such response functions, since experimental data can only be acquired at limited number of input energies. In this paper we will describe a model of the BI CCD developed at MIT to simulate the output of the Chandra flight detectors. We reported on the development of a model for the FI CCDs in.[1] Several other papers[2,3] published by different groups describe similar models of the FI X-ray CCDs.

While many aspects of the modeling of the response to X-rays are very similar for the FI and BI devices, there are several features that differ significantly to justify the development of a separate simulator. The most important of these are loss of charge at the illuminated surface of the BI CCD and significant charge transfer inefficiency (CTI) of the BI devices. Modeling of the X-ray BI CCDs is described in.[3,4] Our model is significantly different from those, most importantly in that it attempts to simulate the physical mechanism of the CTI.

Send correspondence to G.P.
G.P.: E-mail: gyp@space.mit.edu, Telephone: 617 253 7246

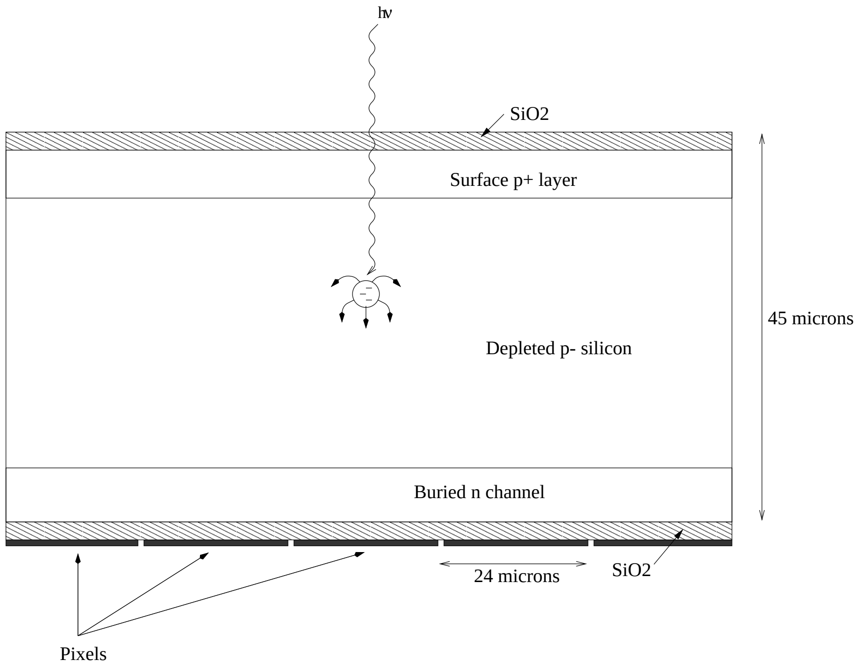

Figure 1. Schematical cross section of a BI CCD.

2. GENERAL DESCRIPTION OF THE MODEL OF THE BACKSIDE ILLUMINATED CCD

Our BI CCD model is based on the Monte-Carlo technique where individual photons of a given energy are thrown onto the surface of the device at random locations, and then the behavior of each photon is traced. The program consists of several distinct blocks. Many of them are very similar or identical to the ones used by our FI simulator.[1] In this paper we will emphasize the features that are different.

The program determines the distance from the surface to the site of photon interaction with silicon, based on the probability of absorption. Exposed surface of the BI CCD is flat and covered by a uniform layer of SiO_2 (a schematic cross section of device structure is shown on Fig. 1), which is much easier to model, compared to the surface of the FI CCD covered by overlapping layers of polysilicon and SiO_2 of different thicknesses and widths. Then the program determines whether flourescence took place. If the answer is yes, the fluorescent photon emitted in a random direction is traced. It can either escape the wafer or to be absorbed. In the absorption case the fluorescent photon is treated separately in the same way as the original photon. For each photon only a small array of 11 x 11 pixels around the interaction site is analyzed. Since we do not process entire CCD frame at once, the program runs very fast and it is practical to simulate millions of photons at each energy.

Then the expansion of the charge cloud and charge losses due to interaction with the surface are calculated. The next step is finding the distribution of charge between the pixels surrounding the photon interaction site.

After that the code simulates charge transfers from the imaging section into frame store, from the frame store into the serial register and serial transfer into the readout node. Each of these transfers produces charge losses due to the traps in the transfer channel. Since every of these transfers has a different speed, different time constants are involved.

Finally, readout noise is added to each pixel and event finding procedure determines which pixel in the analyzed 11 x 11 array has the maximum amplitude. A standard ACIS 3 x 3 event is then written to the output eventlist. If the fluorescent photon formed a separate event, both events are recorded separately.

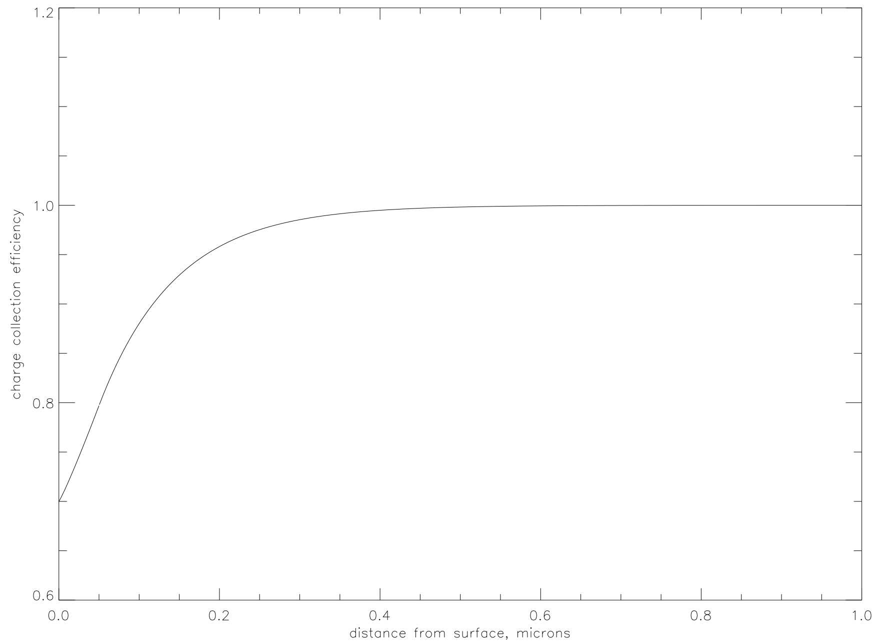

Figure 2. Charge collection efficiency as a function of depth into the silicon.

2.1. Charge collection efficiency

Experimental data taken at low X-ray energies show that energy resolution of the BI CCD stays almost constant below 1 keV. This means that relative deterioration of the Fano-limited resolution is much worse at low energies, where penetration depth of photons is very small. Measurements near the readout node reduced CTI effects and showed that this phenomenon cannot be explained by CTI. This suggests that that it must be caused by recombination processes near the illuminated surface of the device. Low energy photons interact with silicon close to the surface and electron clouds formed there have some fraction of electrons lost to surface recombination. This leads to smaller amount of charge in the collected electron packet and results in broadening of the line, because interaction depth varies for different photons of the same energy.

We tried several different approaches to simulating the low energy line broadening in BI CCD, the most simple and numerically fast result with decent quality of line fitting in a range of energies was achieved when we used a combination of the model described in[5] with charge splitting mechanism between Si and SiO_2 as in our paper.[6] For every charge cloud formed close to the surface the portion of the cloud might be formed inside the SiO_2 layer. According to[5] a different coefficient should be used in order to determine number of electrons formed in silicon dioxide per eV of the photon energy. Once the number of electrons in the cloud inside silicon is determined it is multiplied by a Charge Collection Efficiency (CCE) coefficient which is the following function[5] of the photon depth of penetration into silicon z:

$$CCE = \begin{cases} s + b(z/l)^c, & z \leq l \\ 1 - a\exp(-(z-l)/\tau), & z > l \end{cases} \tag{1}$$

where $a = \frac{(1-s)c\tau}{(c\tau+l)}$ and $b = \frac{(1-s)l}{(c\tau+l)}$. This function combines an exponential decay of the charge loss with a much slower power law at very small distances from the surface. It assumes that every electron packet with total amount of charge Q loses certain fraction of signal depending on the distance of the center of the cloud from the $Si - SiO_2$ interface. The best results in fitting the shape of the response peaks in the wide range of energies were obtained for the following values of the parameters: $s = 0.7, l = 0.05, c = 1.1, \tau = 0.095$. The plot of the resultant CCE as a function of depth z is shown in Fig. 2.

2.2. Charge transfer inefficiency

Charge transfer inefficiency is the most complex part of the simulator. During the initial ground calibration of the BI CCDs it was found that they suffer significant losses of signal charge during the charge transfer. This charge loss was characterized at different photon energies and the results were used to tune the parameters of the simulator.

CTI results from trapping of signal electrons by defects in the transfer channel and their subsequent release into trailing pixels. The amount of charge lost by signal packet of electrons depends on the number of empty traps encountered. The number of empty traps in a given pixel is a function of the time since this particular pixel was occupied by a previous signal packet (so-called "precursor"). The longer the time since the precursor event, the larger the number of traps that will have emptied when the signal packet arrives at the current location, and the larger will be the charge loss (see[7]). This means that CTI improves at higher X-ray flux because the average distance between events gets smaller.

The simulator works on an event by event basis without keeping memory of the entire frame. In order to reflect charge loss dependence on the number of events per frame, for every event a distance to the precursor is determined by a Poisson random number generator with a mean distance corresponding to a specified X-ray flux which is a model input parameter. The distribution of charge in pixels of the precursor event is set equal to that of the prevously simulated photon.

For each of the pixels in the analyzed island all three transfer sequences are simulated: image to frame store transfer, frame store to serial register, and serial register readout. We assume that once the charge packet arrives under the gate it fills all the empty traps in the channel inside the volume it occupies. As soon as the charge packet is transferred under the adjacent gate, the traps start to emit the captured electrons back into the channel. Another assumption is that all electrons emitted by the occupied traps in the channel under two adjacent gates join the packet sitting under the gate between them.

Different portions of the volume of the channel were filled at different times, so each portion has different ratio of empty/filled traps. The calculation of the corresponding volumes is very detailed and keeps track of the time at which each of them started to reemit charge back into the channel. A cartoon showing an expample of these volumes under 3 adjacent gates, and the location of the corresponding 4 precursor pixels with different amount of charge in them, is presented in Fig. 3. This figure shows a signal charge Q_s that is kept under gate G2 and occupies a volume V_s. In order to calculate the emission processes under gate G2 one needs to find the nearest previous signal packet in front of V_s that occupies larger volume than V_s. That volume is V_{prev2}. Notice that the volume V_{prev1} does not play any role in emission under gate G2 or anywhere to the left of it, because all the traps are filled by the larger signal Q_s which erases the memory of the smaller preceeding packet.

The traps inside the volume $(V_{prev2} - V_s)$ were all filled when the packet Q_{prev2} passed the pixel T_{prev2} seconds ago. With exponential reemission of trapped electrons with a time constant τ_e, only $(V_{prev2} - V_s)N_t \exp\left(\frac{-T_{prev2}}{\tau_e}\right)$ traps will be occupied by the time Q_s arrives. Here N_t is volume trap density in the channel.

For the image to frame store transfer we assume that signal charge spends 1/3 of the transfer period under each of the 3 pixel gates. The product of the amount of occupied traps calculated above and $(1 - \exp(\frac{-T/3}{\tau_e}))$ gives the number of electrons Q_{emitG2} reemitted back into the signal packet while it sits under gate G2 from the volume $(V_{prev2} - V_s)$,

$$Q_{emitG2} = (V_{prev1} - V_s)N_t \left(1 - \exp\left(\frac{-T/3}{\tau_e}\right)\right) \exp\left(\frac{-T_{prev1}}{\tau_e}\right). \qquad (2)$$

Exactly the same calculation has to be made for the portion of the volume $(V_{prev4} - V_{prev2})$. Again, the memory of the Q_{prev3} is erased by the following larger packet Q_{prev3}.

During the time under the gate G2 the packet will also collect electrons emitted from the channel under the gate G1 located behind G2. Packet Q_s has just left all the traps in the volume V_s filled under that gate (unless

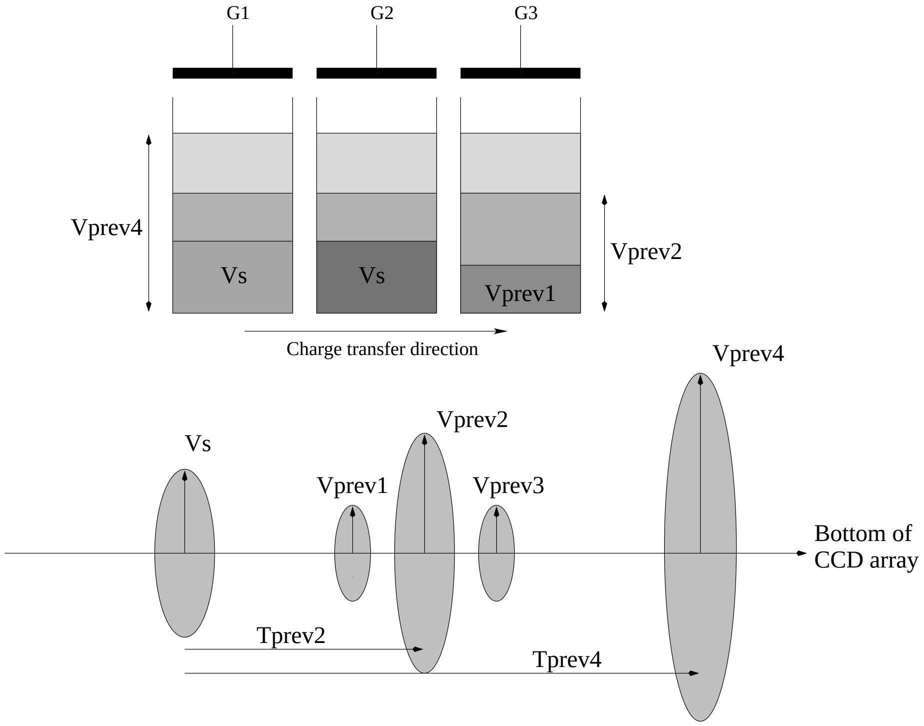

Figure 3. Electron packets under the pixel gates G1, G2, and G3 (top). Location of the packets in the column of the CCD array (bottom).

it is the very first transfer) and traps in the volume $(V_{prev2} - V_s)$ were filled a time $(T_{prev1} + T/3)$ ago. So, one can write an analogous expression for G1:

$$Q_{emitG1} = V_s N_t \left(1 - \exp\left(\frac{-T/3}{\tau_e}\right)\right) + (V_{prev2} - V_s))N_t \exp\left(\frac{-T_{prev2}}{\tau_e}\right)\left(1 - \exp\left(\frac{-T/3}{\tau_e}\right)\right) \tag{3}$$

Again, the corresponding term for $(V_{prev4} - V_{prev2})$ has to be added.

For gate G3 situation is different because the packet Q_s had not been there yet and all the occupied traps inside volume V_{prev1} that were filled a time $(T_{prev1} - T/3)$ ago will emit electrons which will be collected into the potential well under G2. Hence,

$$Q_{emitG3} = V_{prev1} N_t \exp\left(\frac{-(T_{prev1} - T/3)}{\tau_e}\right)\left(1 - \exp\left(\frac{-T/3}{\tau_e}\right)\right) \tag{4}$$

The same calculation is repeated for the portions of the volume $(V_{prev2} - V_{prev1})$ and $(V_{prev4} - V_{prev2})$ where V_{prev4} is the volume occupied by the first packet in front of Q_{prev2} that is larger than Q_{prev2}, and so on, until the first signal packet in the column is reached. All the traps between that packet and the bottom of the array are assumed to be empty.

The next step is to calculate the charge lost by the packet Q_s diring the transfer. When the packet Q_s is transferred forward under the gate G3, it will fill all the empty traps in the volume V_s there. Since traps in the volume V_{prev1} started to reemit later that the rest of volume, they have to be treated separately: $Q_{loss} = Q_{loss}(V_{prev1}) + Q_{loss}(V_s - V_{prev1})$, where

$$Q_{loss}(V_{prev1}) = V_s N_t \left(1 - \exp\left(-\frac{T_{prev1} + T/3}{\tau_e}\right)\right). \tag{5}$$

and

$$Q_{loss}(V_s - V_{prev1}) = (V_s - V_{prev1})N_t \left(1 - exp\left(-\frac{T_{prev2} + T/3}{\tau_e}\right)\right). \tag{6}$$

Subtracting the charge losses and adding the reemitted charge produces the charge packet after one transfer. Three transfers inside one pixel are assumed equivalent and are modeled by multiplying a loss in a single transfer by a factor of 3.

For the slow transfer from the frame store section into the serial register the same formulae are used with correction made to account for the fact that the period here equals $278 \times T_{serial}$ ($T_{serial} = 10\mu s$) and timing diagrams are different for different clocks. Gate G2 keeps signal charge only during interval of $2T_{serial}$ and is closed for the rest of the clock period. The number of vertical transfers during the shift into the serial register for each packet is determined by its y coordinate and hence is not the same for all the pixels. Experimental data show that the line width is broadest for the events closest to the top of the CCD array. In order to reproduce this feature we have added a position dependent noise factor to the charge loss during the frame store to serial transfer.

The serial transfer is calculated in the same way as the vertical image to frame store transfer, except that the transfer period T_{serial} is 4 times shorter.

CTI is a strong function of X-ray energy. The measurements made during the ground calibration over a wide range of energies between 277 eV and 9.9 keV with monochromatic X-rays suggest[8] that it is well described by a power law. In order to reproduce this behavior in the model we introduced an energy-dependent trap density with the functional form derived from the experimental results.[8] These dependencies are different for the vertical and horizontal transfers:

$$N_{tv} = N_{v0}(-5.274 \cdot 10^{-6} + 1.6576 \cdot 10^{-3} E^{-0.657534}) \tag{7}$$

$$N_{th} = N_{h0}(-1.55 \cdot 10^{-5} + 2.8959 \cdot 10^{-3} E^{-0.483}), \tag{8}$$

where E is photon energy expressed in ADU, N_{v0} and N_{h0} are normalization constants. This partly phenomenological approach produced reasonable agreement between experimental and simulated data.

3. COMPARISON TO EXPERIMENT

Before launch all 10 CCD chips were a subject of an intensive ground calibration program and large amount of data were collected using different X-ray sources and spectrometers. These data were used to tune the parameters of the model in a wide range of energies. Data were acquired at a number of X-ray energies corresponding to characteristic emission lines of low-Z elements: O, F, Mg, Al, Si, P, Ti, Mn, Cu, Ge. Since these measurements were implemented with uniform illumination of an entire CCD chip, they were very useful in the process of the parameter adjustments of the CTI portion of the simulator.

For charge collection efficiency modelling the low energy data were most important because charge losses at the surface distort the shape of the response function much more severely when the penetration depth is small. We used the data taken at MIT with HIREFS (High Resolution Erect-Field Spectrometer is described in[9]) and at the synchrotron storage ring BESSY in Berlin to adjust the parameters of the CCE model. Synchrotron data were acquired with a non-flight CCD. Since that chip had significantly better CTI than the flight device, synchrotron data proved to be very useful qualitatively, helping to decouple CTI and surface CCE effects. The model was tuned in such a way that a single set of parameters describes device behavior over the entire energy range. All the simulated results shown below at different enrgies and locations were produced without any additional tuning to match a particular set of data; all the model parameters were exactly the same everywhere.

Comparison of the simulated and experimental data at three different energies and at two different locations on a chip (to account for the CTI effects) is shown on Fig. 4. The line widths near the top of the array are slightly larger The data at 525 eV were taken at MIT with HIREFS grating spectrometer and have noticeable amount of background added to the data. It is mostly caused by scattered light and limits measurement accuracy of the low energy tail of the response. The response near the top of the array is measured using the second order of the dispersed spectrum and shows a first order peak at 212.5 eV; this also contaminates the low energy tail of the response. The model produces some excess on the low energy side of the main peak, but the difference is small.

The data at 1487 eV and 5898 eV were taken in-flight with External Calibration Source. These data have much lower level of background contamination and the agree with the simulation reasonably well.

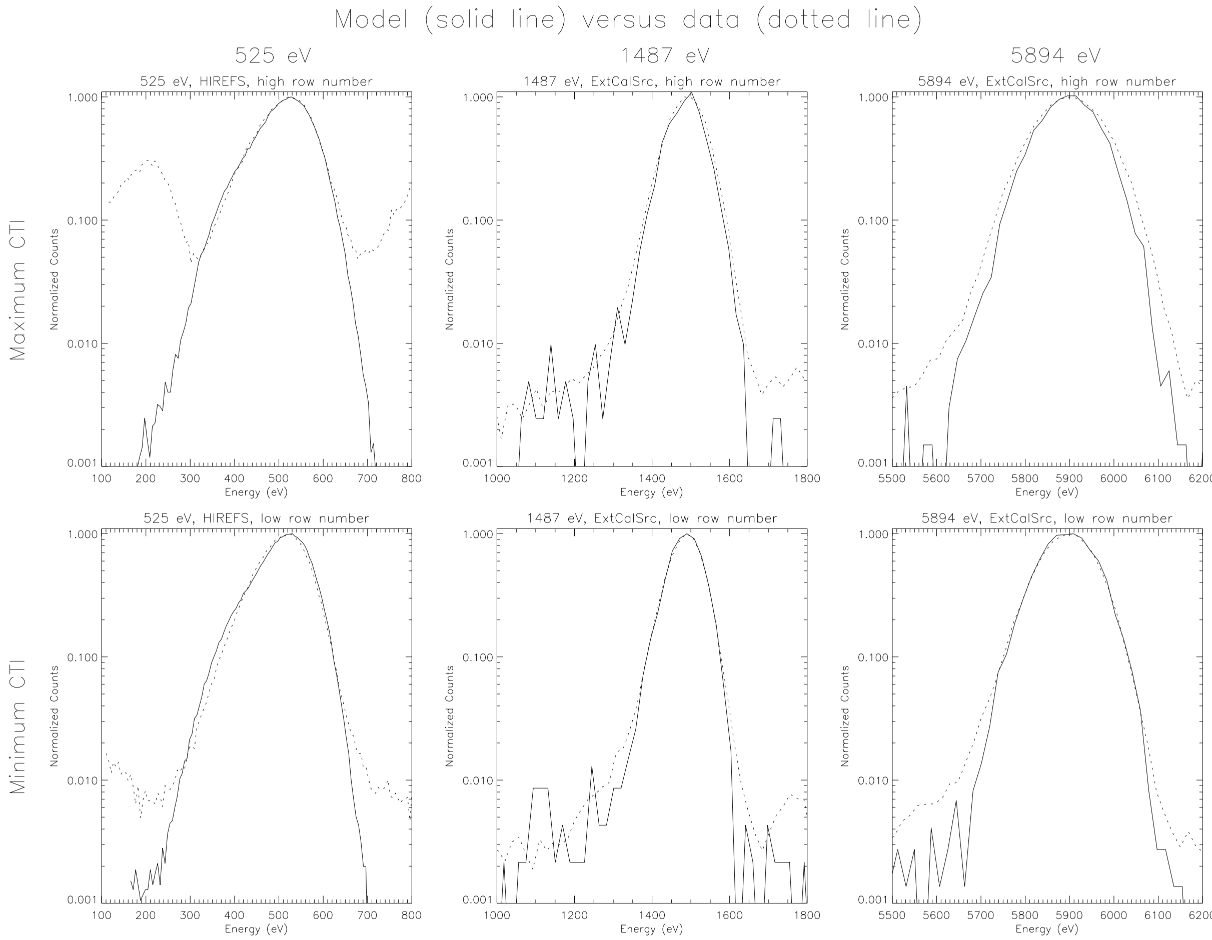

Figure 4. Comparison of simulated response and experimental data at three different energies near the top and the bottom of the CCD array. Data at 525 eV were taken on the ground at MIT with HIREFS spectrometer. Data at 1487 eV (Al K_α line) and 5898 eV (Mn K_α) were taken on-board with ACIS External Calibration Source.

ACKNOWLEDGMENTS

We would like to thank Catherine Grant and Beverly LaMarr for their help with data analysis. This work was funded by NASA through the Chandra X-ray Center.

REFERENCES

1. G. Prigozhin, A. Rasmussen, M. Bautz, and G. Ricker, "A model of the X-ray response of the ACIS CCD," in *EUV, X-ray, and Gamma-ray instrumentation for Astronomy*, Siegmund and Gummin, eds., *Proc. SPIE* **3444**, pp. 267–275, 1998.
2. K. McCarthy, A. Owens, A. Holland, and A. Wells, "Modelling the X-ray response of charge coupled devices," *Nuclear Instruments and Methods in Physics Research A* **362**, pp. 538–546, 1995.
3. L. Townsley, P. Broos, G. Chartas, E. Moskalenko, J. Nousek, and G. Pavlov, "Simulating CCDs for the Chandra Advanced CCD Imaging Spectrometer," *Nuclear Instruments and Methods in Physics Research A* **486**, pp. 716–750, 2002.
4. T. Bootsma, E. van Zwet, A. Brinkman, J. den Herder, L. de Jong, P. de Korte, and S. Olsthoorn, "Synchrotron calibration and response modelling of back-illuminated XMM-RGS CCDs," *Nuclear Instruments and Methods in Physics Research A* **439**, pp. 575–581, 2000.

5. M. Popp, R. Hartmann, H. Soltau, L. Struder, N. Meidinger, P. Holl, N. Krause, and C. von Zanthier, "Modeling the energy response on pn-CCDs in the 0.2-10 keV band," *Nuclear Instruments and Methods in Physics Research A* **439**, pp. 567–574, 2000.
6. G. Prigozhin, S. Jones, M. Bautz, G. Ricker, and S. Kraft, "Physics of the low energy tail in the ACIS CCD. The spectral redistribution function," *Nuclear Instruments and Methods in Physics Research A* **439**, pp. 582–591, 2000.
7. K. Gendreau, G. Prigozhin, R. Huang, and M. Bautz, "A technique to measure trap charachteristics in CCDs using X-rays," *IEEE Transactions on Electron Devices* **42**, pp. 1912–1917, 1995.
8. N. Schulz, "http://space.mit.edu/˜nss/cti_prelaunch.html.".
9. G. Prigozhin, M. Bautz, K. Gendreau, and G. Ricker, "Calibration of X-ray CCDs with an Erect-Field Grating Spectrometer in the 0.2-1.5 keV band," in *EUV, X-ray, and Gamma-ray instrumentation for Astronomy*, Siegmund and Gummin, eds., *Proc. SPIE* **2808**, pp. 260–270, 1996.